Continuum model of confined magnon polaritons in superlattices of antiferromagnets

T. Dumelow and M. C. Oliveros
Departamento de Física, Universidade Federal do Rio Grande do Norte, 59072-970 Natal RN, Brazil
(Received 28 May 1996)

We present a theory of polariton modes in superlattices of antiferromagnetic materials. We apply a continuum approach which models magnon confinement using only the bulk properties of the materials. We assume the modes to be completely pinned at the interfaces, so that the pure modes would take the form of simple sine waves. The expression for the superlattice permeability tensor thus obtained is simple to use and requires only the substitution of the appropriate parameters. We expect the approach to model the effects of confinement accurately at low temperatures provided the superlattice layers are not too thin (a few lattice periods) and the resonances in the constituent layer materials are not very close together. We apply the model to an FeF_2/MnF_2 superlattice, and calculate oblique incidence reflectivity and attenuated total reflection spectra for the anisotropy axis along three different directions. We find that such spectra show a wealth of detail, and are radically affected by the anisotropy direction and by the polarization of the incident light. [S0163-1829(97)00601-2]

I. INTRODUCTION

In recent years high-quality superlattices of antiferromagnet materials have been successfully grown,[1–3] generating considerable interest in the magnon polariton spectra expected from such structures. A number of theoretical studies now exist on this subject.[4–8] In general, the approach has been to use a bulk slab model (in which each constituent layer is considered to retain its bulk properties) usually in the long-wavelength limit in which effective-medium theory may be applied.

Superlattice effective-medium theory,[9–11] initially developed to study electrodynamics of semiconductor superlattices, has proved to be very useful in interpreting far-infrared reflectivity and attenuated total reflection (ATR) measurements on semiconductor superlattices specimens.[12–14] The effective-medium results for bulk slab superlattices can be derived by a simple field-continuity argument[9] or from the transfer-matrix theory[10,15] taking the adequate limit $qL \ll 1$, where L is the superlattice period and q is the magnitude of the superlattice wave vector. The superlattice can then be considered as a single anisotropic medium.

Considering its success in modeling phonon polaritons in semiconductor superlattices, the application of the effective-medium limit[16,17] of the bulk slab model[18] to magnetic superlattices seemed logical. This approach has been used to model bulk and surface magnetostatic modes and polaritons in antiferromagnet/antiferromagnet and antiferromagnet/nonmagnetic superlattices both without[4,6] and with an external applied static magnetic field.[7,8] In the latter case the superlattice permeability is not only anisotropic but also gyrotropic.

The problem with bulk slab theories is that they ignore the effects of the interfaces. In superlattices of antiferromagnets the most prominent of these effects is likely to be that of magnon confinement. If the resonance frequencies in the two constituent antiferromagnet layers are appreciably different, magnon modes will be effectively pinned at the interfaces, so that a bulk description of the constituent layers is not strictly accurate. The resulting ''standing spin waves'' have been observed experimentally in single films[19] of MnF_2 as thick as 1 μm. It appears unlikely that such effects can therefore be ignored in superlattices, even when the layers are relatively thick (hundreds of angstroms). This contrasts with the case for semiconductor superlattices for which the analogous phenomenon of phonon confinement is only important for layers a few lattice units thick.[11]

Although magnon confinement or other microscopically based effects place restrictions on the use of bulk slab models, effective-medium theory, which requires only that $qL \ll 1$, is still relevant. The result is that, in the long-wavelength limit, the superlattice behaves as a single anisotropic medium, as in the bulk slab case. However, a somewhat more sophisticated form of the permeability tensor than that supplied by the bulk slab model is now required. One can take a microscopic approach to this problem by solving all the equations of motion, with a long-range dipolar field included, and applying periodic boundary conditions over the superlattice period. This methodology has been successfully used in the past to model phonon polaritons in short period semiconductor superlattices.[20] Recently Stamps and Camley[21] have taken the same approach in modeling short period (four lattice units in each monolayer) superlattices of easy-plane antiferromagnets. In this case they found the effects of interlayer exchange to be important.

For a superlattice period containing many lattice units, considerable computing power would be needed in applying a microscopic approach to the calculation of superlattice susceptibilities. However, a full microscopic approach may not be necessary in structures of this sort. The present paper is concerned with such cases. It uses a continuum approach that requires only substitution into simple equations while still retaining the effects of confinement. A similar approach has already been applied to phonons in semiconductor superlattices.[22,23] However, we expect the continuum approach to be more applicable to the present case since magnon confinement effects should be observed at longer superlattice periods than should phonon confinement effects.

 © 1997 The American Physical Society

We consider superlattices containing uniaxial antiferromagnet layers of sufficient thickness that the microscopic details at the interfaces are unimportant, and we assume total pinning. This should be reasonable provided the resonant frequencies for the two constituent layers are sufficiently far apart. We take the magnon modes to be totally confined within the individual superlattice monolayers such that the magnetization associated with each mode varies across the layer as a sine wave. At a given frequency, all the confined modes contribute to a local susceptibility to a lesser or greater extent. We calculate the local susceptibility associated with each mode, and sum over all modes. The overall superlattice response is then obtained by averaging the local susceptibility across the superlattice period in a manner consistent with Maxwell's equations, thus leading to an effective-medium permeability tensor.

Most antiferromagnetic resonance frequencies lie in the far-infrared region of 3 to 500 cm^{-1}. Far-infrared Fourier-transform spectroscopy has recently been employed to study magnon polaritons in antiferromagnets[24–26] using essentially the same techniques as previously used on semiconductor superlattices.[22] We therefore expect this spectroscopy to prove very useful in characterizing antiferromagnet superlattice structures in terms of the permeability tensor. In view of this, we have calculated theoretical spectra based on the above superlattice model.

The plan of the paper is as follows. In Sec. II we derive the response of a bulk uniaxial antiferromagnet to a hypothetical driving field varying as $\exp[i(k_z z-\omega t)]$. Later in the paper k_z will be used to represent an effective confinement wave vector within a superlattice layer. In Sec. III we present a study of superlattice fields in the long-wavelength limit $qL \ll 1$. In particular we show that the in-plane **H** component and the out-of-plane **B** component are constant irrespective of any local fluctuations in the permeability across the superlattice period. The superlattice permeabilities are derived in Sec. IV, making use of the bulk susceptibilities from Sec. II and the constant field results from Sec. III. In Sec. V we calculate the permeability tensor for the specific FeF_2/MnF_2 superlattice structure and use it to model far-infrared spectra. Conclusions are presented in Sec. VI.

II. BULK SUSCEPTIBILITIES

When we discuss the superlattice response in Sec. V, we shall consider magnon modes confined within individual superlattice layers. We shall assume that the magnetization associated with each confined mode varies across the layer width as a sine wave, and hence we can assign such a mode an effective confinement wave vector which we shall call k_z.

In this section, we consider the response of a bulk material to a hypothetical driving field varying as $\exp[i(k_z z-\omega t)]$, with the magnetization varying in the same way, as a function of ω and k_z. When we later discuss superlattices, k_z will be used to represent the effective confinement wave vector described above. The magnetization due to individual confined modes within a superlattice layer varies along z as $\sin(k_z z)$, in the same way as the magnetization described in this section. The driving field in a superlattice, however, does not vary in this way (we shall actually be considering responses to constant fields). We show how to correct for this in Sec. IV. We emphasize that we never use k_z as a polariton wave vector; that quantity will have the symbol **q**, and will be introduced in Sec. III.

We derive the response in a uniaxial bulk antiferromagnetic material, having a rutile structure with lattice constants a and c. There is no static external field. The derivation of the susceptibilities is a simple modification of that commonly used to describe the long-wavelength response in an antiferromagnet.[27] Wave-vector dependence is incorporated in a similar manner to the way in which, for instance, Loudon and Pincus[28] describe the dispersion of the magnons themselves.

Consider first the case when the anisotropy axis c is along the wave-vector direction z. We use the torque equation for ions in sublattice i, which has a magnetization $\mathbf{M}_i$:

$$1/\gamma d\mathbf{M}_i/dt=\mathbf{M}_i\times\mathbf{H}_{i,\mathrm{eff}}, \tag{1}$$

where γ is the gyromagnetic ratio and the effective field $\mathbf{H}_{i,\mathrm{eff}}$ is given by

$$\mathbf{H}_{i,\mathrm{eff}}=\mathbf{H}_{i,E}+\mathbf{H}_{i,A}+\mathbf{H}. \tag{2}$$

The quantities on the right-hand side of Eq. (2) represent the exchange, anisotropy, and the driving fields respectively. As is usual practice for antiferromagnets, we ignore the Brooks-Harris field.

In the present case, $\mathbf{H}_{i,A}$ is directed along z, so the z components may be represented as $+H_A$ on sublattice 1 and $-H_A$ on sublattice 2. We consider small oscillations of the magnetization in the xy plane, associated with precessions around the z axis, so that the z components of the magnetizations and the exchange fields may similarly be represented as the static values $+M$ and $+H_E$, respectively, on sublattice 1 and $-M$ and $-H_E$, respectively, on sublattice 2.

We assume that the exchange field acting on ions in sublattice 1 is due only to nearest neighbors, and that the magnetizations vary as $\exp[i(k_z z-\omega t)]$. The x component of this exchange field is then given by

$$\begin{aligned}H_{ix,E}&=-1/2[\exp(ik_z c/2)+\exp(-ik_z c/2)]H_E(M_{2x}/M)\\&=-H_E(M_{2x}/M)\cos(k_z c/2),\end{aligned} \tag{3}$$

where c is the lattice parameter along the anisotropy axis. Equivalent equations apply for the y component and the other sublattice.

We now substitute for the appropriate components of the **H** fields used in Eq. (2), and write the x and y components of Eq. (1) as

$$-i(\omega/\gamma)M_{1x}=(H_A+H_E+H_z)M_{1y}-[-H_E M_{2y}\cos(k_z c/2)+H_y M], \tag{4}$$

$$-i(\omega/\gamma)M_{1y}=-(H_A+H_E+H_z)M_{1x}+[-H_E M_{2x}\cos(k_z c/2)+H_x M], \tag{5}$$

$$-i(\omega/\gamma)M_{2x}=(-H_A-H_E+H_z)M_{2y}-[H_E M_{1y}\cos(k_z c/2)-H_y M], \tag{6}$$

$$-i(\omega/\gamma)M_{2y} = -(-H_A - H_E + H_z)M_{2x} + [H_E M_{1x}\cos(k_z c/2) - H_x M]. \quad (7)$$

Equations (4)–(7) may be solved to get the various bulk susceptibilities as a function of k_z. χ_x^{bulk} is given by $(M_{1x}+M_{2x})/H_x$ and so on. The results are

$$\chi_x^{\text{bulk}}(k_z) = \chi_y^{\text{bulk}}(k_z) = \frac{S_c(k_z)}{\omega_{Tc}^2(k_z) - \omega^2}, \quad (8)$$

$$\chi_z^{\text{bulk}}(k_z) = 0, \quad (9)$$

where $\omega_{Tc}(k_z)$ is the transverse resonance frequency and is given by

$$\omega_{Tc}^2(k_z) = \gamma^2 H_A(H_A + 2H_E) + H_E^2\gamma^2 \sin^2(k_z c/2) \quad (10)$$

and $S_c(k_z)$ is the associated oscillator strength, given by

$$S_c(k_z) = 2M\gamma^2[H_A + H_E - H_E\cos(k_z c/2)]. \quad (11)$$

$\chi_x^{\text{bulk}}(k_z)$ should, of course, strictly be written as $\chi_x^{\text{bulk}}(k_z,\omega)$, with similar modifications for the other components, but we keep the shorter notation for simplicity.

An equivalent approach may be applied for the anisotropy axis along x. In this case the results are

$$\chi_x^{\text{bulk}}(k_z) = 0, \quad (12)$$

$$\chi_y^{\text{bulk}}(k_z) = \chi_z^{\text{bulk}}(k_z) = \frac{S_a(k_z)}{\omega_{Ta}^2(k_z) - \omega^2}. \quad (13)$$

$\omega_{Ta}(k_z)$ and $S_a(k_z)$ are given by the same expressions as for $\omega_{Tc}(k_z)$ in Eq. (10) and $S_c(k_z)$ in Eq. (11) respectively, except that in each case the lattice parameter c is replaced by the lattice parameter a. For the anisotropy axis along y, one need simply swap the susceptibilities $\chi_x^{\text{bulk}}(k_z)$ and $\chi_y^{\text{bulk}}(k_z)$ in Eqs. (12) and (13).

Equations (9)–(11) give responses to **H** fields. In the analysis that follows, we shall use the results for $\chi_x^{\text{bulk}}(k_z)$ and $\chi_y^{\text{bulk}}(k_z)$. However, for reasons that will become clear later, it is useful to transform $\chi_z^{\text{bulk}}(k_z)$ into a response to a **B** field. For the anisotropy axis along z, of course, this response, which we shall call $\psi_z^{\text{bulk}}(k_z)$, will be zero. For the anisotropy axis along x or y, however, we can transform Eq. (13) as

$$\psi_z^{\text{bulk}}(k_z) = \frac{M_{1z}+M_{2z}}{H_z + 4\pi(M_{1z}+M_{2z})} = \frac{S_a(k_z)}{\omega_{La}^2(k_z) - \omega^2}, \quad (14)$$

where $\omega_{La}(k_z)$ is a longitudinal resonance frequency given by

$$\omega_{La}^2(k_z) = \omega_{Ta}^2(k_z) + 4\pi S_a(k_z) \quad (15)$$

in agreement with Loudon and Pincus.[28]

The above susceptibilities will be used as a basis for determining superlattice responses. Note that we do not immediately apply Maxwell's equations to these results, as we would to model polaritons in the bulk antiferromagnet,[29] because the superlattice fields used later in the paper will not be of the same form as described above.

III. SUPERLATTICE FIELDS IN THE LONG-WAVELENGTH LIMIT

We are interested in the superlattice response in the regime for which the polariton wavelengths are much larger than the superlattice period. Typically the free space wavelengths are greater than 100 μm, and since we consider superlattices with periods of a few hundred angstroms or less, this criterion is easily satisfied. The effective-medium model used here relies on the fact that in the long-wavelength regime the in-plane component of the **H** field and the out-of-plane (z) component of the **B** field are constant over the superlattice period. This assumption has been widely applied to bulk slab superlattices[4,6–8] and to structures which can be considered in terms of discrete planes.[21,30] In both such cases the result is fairly obvious from the field boundary conditions. In this section we consider the fields involved and present a simple proof that the required components are indeed constant regardless of any local variations in the susceptibility, along the growth direction, within the superlattice period. An analogous proof, in terms of **E** and **D** fields, is presented elsewhere.[23]

In a superlattice structure in which the lattice is homogeneous in the xy plane but periodic in the z direction, the microscopic fields $\boldsymbol{\mathcal{F}}(\mathbf{r},t)$ follow a Bloch form

$$\boldsymbol{\mathcal{F}}(\mathbf{r},t) = \mathbf{F}(z)\exp[i(\mathbf{q}\cdot\mathbf{r} - \omega t)], \quad (16)$$

where $\mathbf{q}$ is a macroscopic wave vector and

$$\mathbf{F}(z+L) = \mathbf{F}(z) \quad (17)$$

with L the superlattice period. In the long-wavelength limit it is also appropriate to consider macroscopic fields $\boldsymbol{\mathcal{F}}(\mathbf{r},t)$ which also follow the Bloch form

$$\bar{\boldsymbol{\mathcal{F}}}(\mathbf{r},t) = \overline{\mathbf{F}}\exp[i(\mathbf{q}\cdot\mathbf{r} - \omega t)], \quad (18)$$

where $\overline{\mathbf{F}}$ is the average of $\mathbf{F}(z)$ over the superlattice period. This definition ensures that so long as the microscopic fields obey Maxwell's equations, so do the macroscopic fields.

We now apply Maxwell's Equation $\boldsymbol{\nabla}\cdot\boldsymbol{\mathcal{B}} = 0$ to Eq. (16):

$$i\mathbf{q}\cdot\mathbf{B} + \partial B_z/\partial z = 0. \quad (19)$$

The first term in this equation is of order qB. In the long-wavelength limit we have $qL \ll 1$, so that $\partial B_z/\partial z \ll B/L$, i.e., B_z is effectively constant over the superlattice period.

In order to show that H_x and H_y are constant we apply $\boldsymbol{\nabla}\times\boldsymbol{\mathcal{H}} = (1/c)\partial\boldsymbol{\mathcal{D}}/\partial t$ to Eq. (16):

$$i\mathbf{q}\times\mathbf{H} - \mathbf{e}_x\partial H_y/\partial z + \mathbf{e}_y\partial H_x/\partial z = -i(\omega/c)\mathbf{D}, \quad (20)$$

where $\mathbf{e}_x$ and $\mathbf{e}_y$ are unit vectors. We now compare Eq. (20) with the result of applying $\boldsymbol{\nabla}\times\boldsymbol{\mathcal{H}} = (1/c)\partial\boldsymbol{\mathcal{D}}/\partial t$ to the macroscopic field equation (18):

$$i\mathbf{q}\times\overline{\mathbf{H}} = -i(\omega/c)\overline{\mathbf{D}}. \quad (21)$$

Now the macroscopic fields $\overline{\mathbf{H}}$ and $\overline{\mathbf{D}}$ will be of the same order as the microscopic fields **H** and **D**. Comparison of the two equations (20) and (21) therefore shows that all the terms in Eq. (20) should, for arbitrary polarization and wave-vector directions, be of the same order (with the exception that if the anisotropy is along x or y then either $\partial H_x/\partial z$ or $\partial H_y/\partial z$ will be identically zero, leaving the remaining terms

of the same order as one another). Hence, in the long-wavelength limit $qL \ll 1$, using the same argument as for the B_z fields, we have both $\partial H_x/\partial z$ and $\partial H_y/\partial z$ much less than H/L, i.e., both H_x and H_y are effectively constant over the superlattice period. In determining the superlattice susceptibilities, it will prove convenient to consider responses to the constant fields H_x, H_y, and B_z.

IV. SUPERLATTICE PERMEABILITIES

We consider first superlattice responses along the x direction. As explained in the previous section, H_x will be constant in the long-wavelength limit, so we simply consider responses to this constant field. The magnetization, in contrast, will vary along z, so it is useful to consider a local susceptibility $\chi_x(z)$:

$$M_x(z) = H_x \chi_x(z). \tag{22}$$

We initially consider the susceptibility within layer 1 of the superlattice period, occupying the space $0 \leqslant z \leqslant d_1$, the layer thickness d_1 corresponding to n_1 lattice units. Of course, if the anisotropy is along x, $\chi_x(z)$ is always zero, and the problem is trivial. For anisotropy along y or z, we assume total pinning at the interfaces, so that there is a series of n_1 confined magnon modes, each making a contribution, varying as $\sin(m\pi z/d_1)$, to the magnetization. m is the order of the mode and corresponds to the number of half-wavelengths confined within the layer. Each confined mode makes a similar contribution to the local susceptibility since, from Eq. (22), this varies in the same way as the magnetization:

$$\chi_x(z) = \sum_{m}^{n_1} \varphi_{1xm} \sin(m\pi z/d_1), \tag{23}$$

where φ_{1xm} is a susceptibility associated with the mth confined mode in layer 1. We can consider each confined mode as having an associated confinement wave vector k_z $(=m\pi/d_1)$ which determines the resonance frequency according to, for instance, Eq. (10). The associated susceptibility should have a pole at this frequency, and in general take the same form as the bulk susceptibility $\chi_{1x}^{\text{bulk}}(k_z)$ derived in Sec. II. We thus have

$$\varphi_{1xm} = c_m \chi_{1x}^{\text{bulk}}(k_z = m\pi/d_1). \tag{24}$$

The coefficient c_m, which depends only on mode order m, determines the relationship between the response to a constant H_x field, as used here, and the response to one along z varying as $\exp(ik_z z)$, as used to define $\chi_{1x}^{\text{bulk}}(k_z)$. Formally, $H_x c_m$ is the Fourier coefficient of the component of H_x that varies in the same way as the mth mode magnetization. c_m can therefore be determined by resolving H_x into Fourier components over the layer width. Here we derive an expression for c_m in a somewhat more physical (but slightly less rigorous) way by considering the susceptibility in the limit when d_1 is very large. Both methods lead to the same result.

When layer 1 is sufficiently wide, the layer material retains its bulk properties, and $\chi_x(z)$ is a constant equal to $\chi_{1x}^{\text{bulk}}(k_z = 0)$ over the layer width. However, over the range $0 \leqslant z \leqslant d_1$, we can use the identity

$$\frac{4}{\pi} \sum_{m\ \text{odd}}^{\infty} \frac{1}{m} \sin(m\pi z/d_1) = 1 \tag{25}$$

to express $\chi_x(z)$ as

$$\chi_x(z) = \chi_{1x}^{\text{bulk}}(k_z = 0)\, \frac{4}{\pi} \sum_{m\ \text{odd}}^{\infty} \frac{1}{m} \sin(m\pi z/d_1), \tag{26}$$

i.e., we are expressing the constant susceptibility as a Fourier summation of confined modes. Equation (26) can be seen to be equivalent to the wide layer limit (in which $k_z \to 0$ for the dominant modes) of Eqs. (23) and (24) if we make the substitutions

$$c_m = 4/\pi m, \quad m \ \text{odd},$$

$$c_m = 0, \quad m \ \text{even}, \tag{27}$$

thus giving us the necessary expressions for the coefficients c_m. Note that the even order modes do not contribute to the susceptibility—this is physically reasonable because such modes have no overall dipole moment. We also note that the local susceptibility obtained upon substituting Eqs. (24) and (27) into Eq. (23), and using the bulk susceptibility given by Eq. (8), is exactly the same as obtained for a single thin antiferromagnetic film with anisotropy along z by Orbach and Pincus[31] without using the bulk susceptibility.

In order to get the overall response in the superlattice, we must make the appropriate averages across the superlattice period. Over layer 1 we substitute Eqs. (24) and (27) into Eq. (23), and perform the averaging operation

$$\overline{\chi_{1x}} = \frac{1}{d_1} \int_0^{d_1} \chi_x(z)\, dz = \sum_{m\ \text{odd}}^{n_1} \frac{8\chi_{1x}^{\text{bulk}}(k_z = m\pi/d_1)}{\pi^2 m^2}. \tag{28}$$

If we do the same over layer 2 we can then get an overall permeability component μ_{xx} for the superlattice by averaging over the two layer types, in a similar manner to the procedure used in bulk slab models:[4]

$$\mu_{xx} = 1 + 4\pi \frac{d_1 \overline{\chi_{1x}} + d_2 \overline{\chi_{2x}}}{d_1 + d_2}. \tag{29}$$

μ_{yy} can be obtained in the same way as μ_{xx}. In order to obtain μ_{zz}, however, we consider the response to a constant B_z field. We can then consider a local response to this field $\psi_z(z)$. A similar analysis to the above then gives an average response over layer 1 of

$$\overline{\psi_{1z}} = \sum_{m\ \text{odd}}^{n_1} \frac{8\psi_{1z}^{\text{bulk}}(k_z = m\pi/d_1)}{\pi^2 m^2} \tag{30}$$

with a similar result for layer 2. The responses can be averaged over the two layers, leading to a superlattice permeability of the form

$$\frac{1}{\mu_{zz}} = 1 - 4\pi \frac{d_1 \overline{\psi_{1z}} + d_2 \overline{\psi_{2z}}}{d_1 + d_2}. \tag{31}$$

Thus it can be seen that the expressions needed to determine the superlattice permeability components are very simple ones, requiring only substitution into Eqs. (28)–(31). In this

paper we make use of the bulk susceptibilities $\chi_x^{\text{bulk}}(k_z)$, $\chi_y^{\text{bulk}}(k_z)$, and $\psi_z^{\text{bulk}}(k_z)$ derived in Sec. II. However, the analysis presented in the present section does not depend on any particular model for the bulk susceptibilities, and more sophisticated models (e.g., including next-nearest-neighbor terms) or models for different structures could equally well be used.

V. CALCULATED RESULTS

We now calculate the permeability tensor for a specific superlattice structure and use it to model far-infrared spectra. All results shown in this paper are for $(FeF_2)_{30}/(MnF_2)_{15}$ superlattices, where the subscript on each bracketed component represents the number of lattice units of that component within a superlattice layer (each superlattice period is therefore equivalent to a chain of 60 Fe^{2+} spins followed by a chain of 30 Mn^{2+} spins). We use the same FeF_2 parameters as used in recent far-infrared spectroscopic investigations[24–26] at 4.2 K: $M=0.056$ T, $H_A=19.745$ T, $H_E=53.313$ T, and $\gamma=1.05$ cm^{-1}/T, corresponding to a bulk resonance frequency of $\omega_r=52.45$ cm^{-1}. For MnF_2 we use the values[32–34] $M=0.06$ T, $H_A=0.787$ T, $H_E=53.0$ T, and $\gamma=0.975$ cm^{-1}/T, corresponding to a bulk resonance frequency of $\omega_r=8.94$ cm^{-1}.

Before examining the results of the calculations, we briefly discuss the applicability of the continuum model, with particular regard to the assumption of strong pinning at the interfaces, to the present case. We are not aware of any microscopic calculations for this type of system for comparison. However, we may usefully consider the calculations of Stamps and Camley[21] for a bilayer of two easy-plane antiferromagnets and those of Hinchey and Mills[35] for a superlattice of a ferromagnet with an antiferromagnet similar to MnF_2. Both these examples show well separated resonances, as in the FeF_2/MnF_2 case considered here. We would expect pinning in our example to be similar to that reported in the two microscopic calculations. In fact, it may well be greater, due to the high FeF_2 anisotropy.

The Stamps and Camley paper shows mode amplitudes for a bilayer of two easy-plane antiferromagnets (with some in-plane uniaxial anisotropy included), each of width four spins. For an exchange field across the interface comparable to that in the individual layers, the pinning is seen to be very strong. Even though, for each magnon mode, a small tail can be seen to extend into the nonresonant layer, it does not appear to continue beyond the first spin of that layer. The Hinchey and Mills paper does not show mode amplitudes explicitly, so the degree of pinning cannot be observed directly. However, it does show the dispersion curve corresponding to the lowest antiferromagnet magnon mode in an antiferromagnet/ferromagnet superlattice. For a superlattice period consisting of only four spins of antiferromagnet and four spins of ferromagnet, the magnon mode is almost dispersionless—a classic indication of mode confinement (a similar result is also seen for the ferromagnet modes). Furthermore, the affiliated confinement shift agrees, within 20%, with that of the resonance associated with Eq. (24).

The two examples quoted above suggest that, in our FeF_2/MnF_2 system, penetration into the nonresonant layer is unlikely to extend beyond about one spin. Although this may have a significant effect on the thin layer results discussed in the two microscopic examples, it should have a negligible effect on the wide layers considered here. The use of the continuum model in this case therefore seems well justified.

As an example of the type of spectrum we should expect to see in an $(FeF_2)_{30}/(MnF_2)_{15}$ superlattice, Fig. 1 shows our calculated s-polarization spectrum for 5 μm of superlattice, with the anisotropy axis within each layer along y, deposited on a semi-infinite ZnF_2 substrate. The angle of incidence is 60°, and the plane of incidence is xz, with z normal to the layers. We have included a damping term into the permeabilities using the standard substitution $\omega^2 \rightarrow \omega^2 + i\omega\Gamma$, where Γ is the magnon damping term. Here we use the experimentally observed values[24–26,33] of $\Gamma=0.05$ cm^{-1} for FeF_2 and $\Gamma=0.0007$ cm^{-1} for MnF_2. We also need to include the dielectric response of the substrate and superlattice. We use a value of $\varepsilon=8.0$ for the ZnF_2 substrate.[7] For the superlattice components we take dielectric constants[24–26,33,36] of 5.5 for both FeF_2 and MnF_2. Bulk slab effective-medium theory[9,10] may be used to work out the superlattice dielectric tensor components, but since, in this case, the dielectric constants of the two materials are equal we simply end up with components $\varepsilon_{xx}=\varepsilon_{yy}=\varepsilon_{zz}=5.5$. Note that we retain these quantities as explicit tensor components for the rest of paper, since the isotropy of the superlattice dielectric tensor is simply a consequence of the parameters of the chosen materials, and is not general. Strictly speaking, the dielectric tensor of MnF_2 is itself uniaxial,[7] but this makes a very small difference to the final spectra and it is a trivial matter to incorporate this change into the bulk slab effective-medium expressions.[7] Using the calculated permeability and dielectric tensors, we have worked out the reflectivity utilizing standard transfer-matrix techniques.[22,37]

Figure 1(a) shows the reflectivity spectrum over the entire magnon range. Immediately one can see that there is a large amount of structure due to mode confinement. MnF_2 confined modes occur in the range 10–55 cm^{-1}, and FeF_2 modes occur in the range 50–80 cm^{-1}. In each case the low-order modes are at the low-frequency end of the range. In Fig. 1(b) we show an expansion of the range 51–57 cm^{-1}, which is dominated by features due the lower order FeF_2 modes. The FeF_2 damping is 0.05 cm^{-1} and the width of the resulting features is of this order. The spectrum also shows features due to high-order MnF_2 modes. We have used a much smaller damping (0.0007 cm^{-1}) for MnF_2 and the features appear as ''spikes'' on the spectrum. However, there are a number of reasons why we do not expect to see such MnF_2 features in practice. Firstly, the associated modes are very weak compared to the FeF_2 modes; they are about two orders of magnitude weaker than that of the first FeF_2 mode. Secondly, the model is not designed to describe accurately the behavior of these high-order modes, which may in practice be subsumed into the much stronger FeF_2 modes at around the same frequency. Thirdly, the use of bulk damping parameters for such modes is likely to be unrealistic. It is a feature of confined phonon modes that higher-order modes tend to get damped out,[20] and we expect the same effect here. In addition we note the comments of Lui and co-workers[19,38] that antiferromagnetic resonance in MnF_2 films one to two orders of magnitude thicker than those considered here can only be observed on ultrahigh-quality samples. Due to the

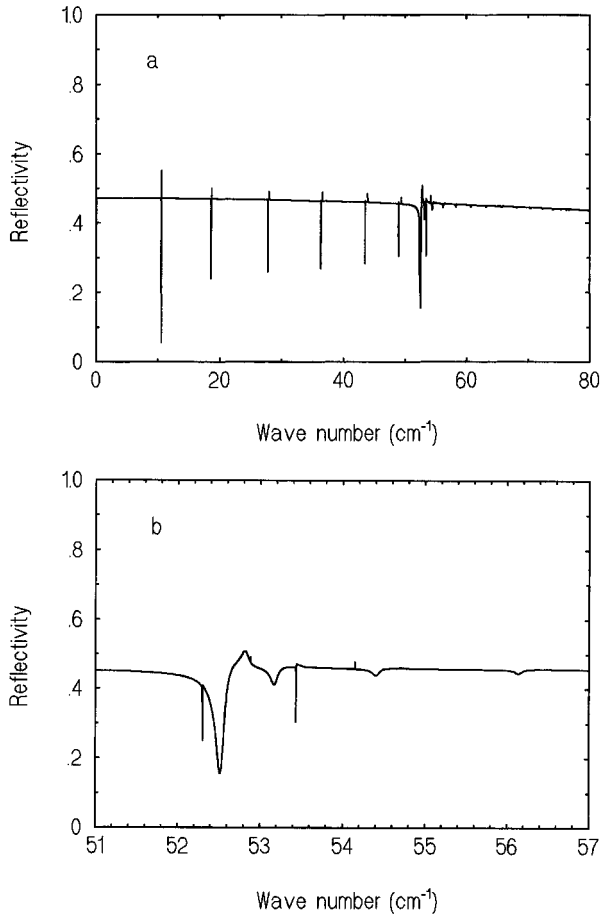

FIG. 1. Calculated 60° oblique incidence s-polarized reflectivity spectrum of 5 μm of $(FeF_2)_{30}/(MnF_2)_{15}$ superlattice deposited on a semi-infinite ZnF_2 substrate. The anisotropy axis is along y.

much lower anisotropy of MnF_2, the MnF_2 modes are in general much weaker, and hence narrower, than the FeF_2 modes. Thus a small amount of inhomogeneity within the MnF_2 layers is likely to damp out the modes, and difficulty may be encountered in observing any superlattice MnF_2 features, even those associated with low-order modes.

For the rest of the paper we concentrate on features associated with FeF_2 magnons in the range 52.4–53.6 cm^{-1}, i.e., in the region of the lowest order modes. For the reasons outlined above, and to simplify our discussion of the spectral features, we have removed the contributions of the high-order MnF_2 modes which fall in this region. We present the three principal components of the undamped permeability tensor in Fig. 2. The case illustrated is for the anisotropy axes along y, as in the example given in Fig. 1. To model the case for anisotropy along x one would simply exchange the x and y components. For anisotropy along z, both μ_{xx} and μ_{yy} would have the same form as μ_{xx} in the case illustrated, with μ_{zz} equal to 1.

We have labeled the frequencies of the odd-index confined transverse and longitudinal confined magnons (for propagation along z) as ω_{Tm} and ω_{Lm}, respectively. Here the index m is the mode order for the FeF_2 layer, and represents the number of half wavelengths confined within that layer. Thus, for the case illustrated, using the terminology in Sec. II, ω_{Tm} is equal to $\omega_{Ta}(k_z = m\pi/d_1)$ and ω_{Lm} is equal to

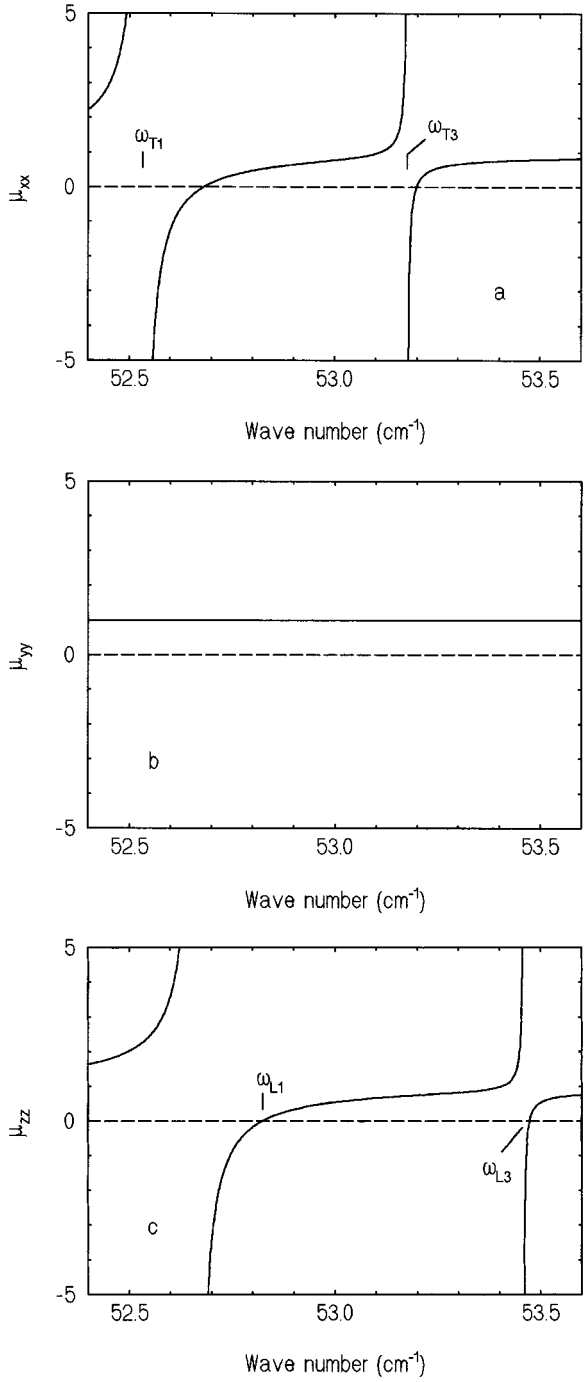

FIG. 2. Undamped permeability tensor components for a superlattice with the anisotropy axis along y. (a) μ_{xx}, (b) μ_{yy}, (c) μ_{zz}.

$\omega_{La}(k_z = m\pi/d_1)$ where d_1 is the thickness of the FeF_2 layer. We see that, ignoring the absence of any response along the anisotropy direction (corresponding to a permeability component equal to 1), μ_{xx} and μ_{yy} have poles at the odd-index confined transverse mode frequencies whereas μ_{zz} has zeroes at the odd-index confined longitudinal mode frequencies. This is analogous to the dielectric tensor results for superlattice confined phonons.[39]

Figure 3 shows the calculated s- and p-polarized reflectivity spectra, in the restricted frequency range discussed above, for superlattices with the anisotropy axis directed along each of the three axes x, y, and z. In all these spectra

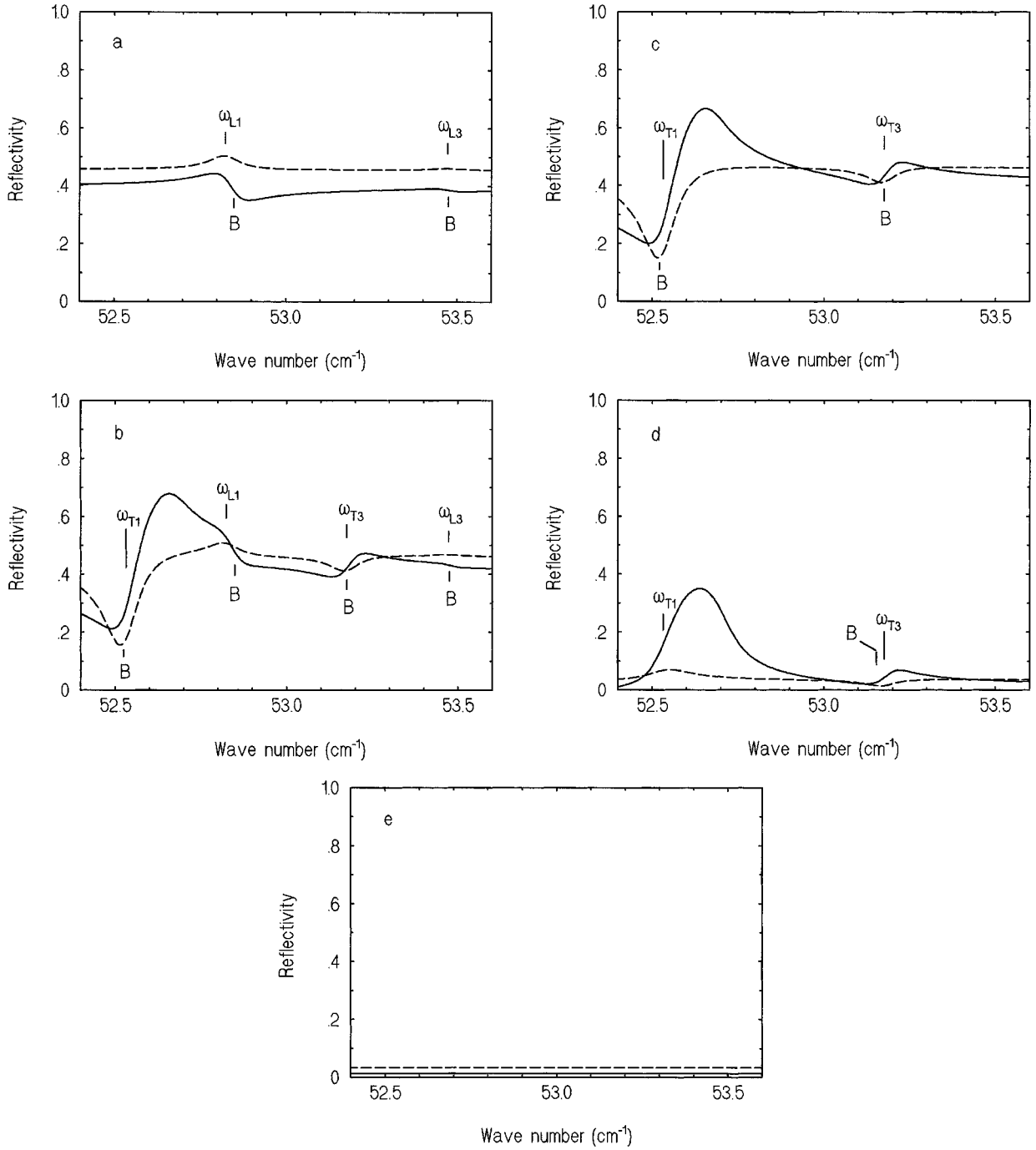

FIG. 3. Calculated 60° oblique incidence reflectivity spectra of (—) a semi-infinite superlattice and (– – – –) 0.5 μm of superlattice deposited on a semi-infinite substrate. (a) *s* polarization, anisotropy along *x*, (b) *s* polarization, anisotropy along *y*, (c) *s* polarization, anisotropy along *z*, (d) *p* polarization, anisotropy along *x* or *z*, (e) *p* polarization, anisotropy along *y*.

the plane of incidence is *xz*, with *z* normal to the surface and the angle of incidence is 60°, as in Fig. 1. Note that the superlattice used for anisotropy along *x* and along *y* would be the same—one would simply have to rotate the sample. To get anisotropy along *z*, however, one would have to grow a different superlattice using a different substrate orientation. Results are shown for both semi-infinite superlattices (although such samples are not likely to be encountered in practice) and superlattices deposited on ZnF_2 substrates.

We concentrate first on the *s*-polarization results. We immediately see that the anisotropy direction fundamentally affects the form of the observed spectra. In *s* polarization the magnetic component of the electromagnetic (EM) field has components along *x* and *z*, and therefore interacts with both these components of the permeability; μ_{yy} never enters the calculation. In addition, however, it should be noted that there is no response along the anisotropy direction. For anisotropy along *x*, therefore, only μ_{zz} contributes to the interaction, and features show up around the zeroes in this component. Similarly, for anisotropy along *z*, there are features associated with poles in μ_{xx}, but none associated with μ_{zz}. For anisotropy along *y*, there is interaction with both μ_{xx} and

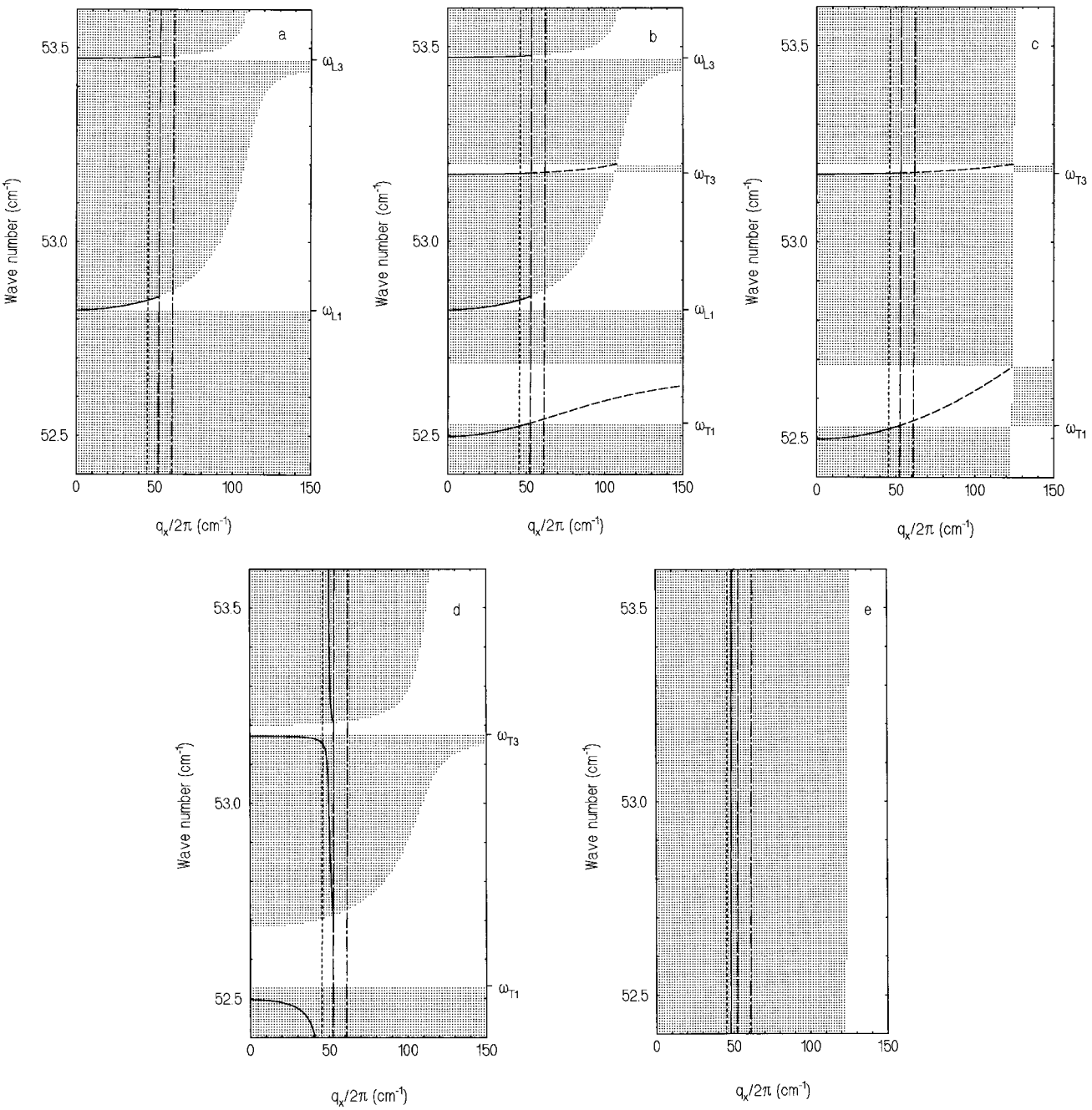

FIG. 4. Brewster mode dispersion curves (—), surface polariton dispersion curves (– – – –), and bulk continua (shaded area) for a semi-infinite superlattice in contact with vacuum. (a) *s* polarization, anisotropy along *x*, (b) *s* polarization, anisotropy along *y*, (c) *s* polarization, anisotropy along *z*, (d) *p* polarization, anisotropy along *x* or *z*, (e) *p* polarization, anisotropy along *y*. The near-vertical scan lines are (---------) 60° scan line for reflectivity from vacuum, (— — —) vacuum light line, and (—·—·—) 20° scan line for silicon ATR.

μ_{zz}, and the spectra show features associated with both components.

The above shows which component we expect to be important in which spectrum. In order to understand the spectra in terms of dips and peaks we consider the results for semi-infinite superlattices in more detail. Here the *s*-polarization reflectivity is given by **rr*** where the complex reflection coefficient **r** is, for a nonmagnetic, isotropic medium of incidence, equal to

$$\mathbf{r}=\frac{q_{1z}\mu_{xx}-q_{2z}}{q_{1z}\mu_{xx}+q_{2z}}. \tag{32}$$

Layer 1 is the incident medium and layer 2 is the superlattice. The wave-vector components q_{1z} and q_{2z} in the two media are given by

$$q_{1z}^2=(\omega/c)^2\varepsilon_1-q_x^2, \tag{33}$$

$$q_{2z}^2=(\omega/c)^2\varepsilon_{yy}\mu_{xx}-q_x^2\mu_{xx}/\mu_{zz}, \tag{34}$$

where ε_1 is the dielectric constant in the incident layer (=1 for vacuum), and ε_{yy} is the appropriate component of the dielectric tensor in the superlattice. The wave-vector compo-

nent q_x is continuous throughout the structure, and is determined by the angle of incidence θ:

$$q_x=(\omega/c)\varepsilon_1^{1/2}\sin\theta. \tag{35}$$

If we ignore damping contributions, q_{2z} is either pure real or pure imaginary. If it is real some radiation will propagate into the sample, and the reflectivity will be less than 1. If, on the other hand, it is imaginary, the reflectivity will be 1. This can be seen in the plots in Fig. 4. Here the shaded regions (the bulk continua) correspond to q_{2z} real and the unshaded regions (the forbidden gaps) to q_{2z} imaginary. Reflectivity experiments can be performed in the region to the left of the grazing incidence vacuum light line $q_x=\omega/c$ [setting ε_1 equal to 1 and θ equal to 90° in Eq. (35)], and an incident angle of 60° corresponds to scan line $q_x=(\omega/c)\sin 60°$. Thus, in the absence of damping, the reflectivity should be 1 at frequencies at which the scan line falls in a forbidden gap (generally just above either ω_{Tm} or ω_{Lm}), and less than 1 elsewhere. If damping is included, the features are somewhat smoothed out, but nevertheless the calculated spectra show peaks in the reflectivity in the region of the forbidden gaps shown in Fig. 4.

Note that in the present example the high reflectivity regions are always just above either ω_{Tm} or ω_{Lm} frequencies. This is not always the case. If, for instance, ω_{T3} were to fall below ω_{L1}, as would happen if the FeF_2 layers were wider, the appearance of the spectrum would be somewhat different. A similar effect associated with phonons in semiconductor superlattices is described in some detail elsewhere.[40]

The above analysis explains the peaks in the reflectivity spectra. In order to discuss the dips we assume zero damping and look for the condition for zero reflectivity. We therefore set the top line of Eq. (32) equal to zero. This results in the equation

$$q_x^2=\frac{\omega^2}{c^2}\,\frac{\varepsilon_{yy}-\varepsilon_1\mu_{xx}}{1/\mu_{zz}-\mu_{xx}}. \tag{36}$$

This is the s-polarization Brewster mode condition, and the corresponding dispersion curves are plotted as solid lines in Figs. 4(a)–4(c). Thus dips in the reflectivity should be seen where these dispersion curves intersect with the scan line (just below ω_{Tm} frequencies or just above ω_{Lm} frequencies). The frequencies of these intersections are marked B in the spectra in Fig. 3, and dips are indeed observed around these frequencies. However, due to the effects of damping, the reflectivity does not drop to zero and the calculated minima do not exactly coincide with the marked frequencies. The fact that the Brewster mode frequencies are generally near to bulk continuum edges means that, in the undamped case, there should be adjacent high and low reflectivity regions—this effect is somewhat smoothed out by damping and the resulting appearance is that the high and low reflectivity regions have been pushed apart. Nevertheless, the presence of Brewster modes does produce distinctive features that should help in interpreting experimental spectra.

In the case of the superlattice film on a substrate, most of the basic features are retained. However, some of the Brewster modes effectively disappear. This is not surprising, because the whole basis of calculating the Brewster mode condition is that all the energy is transmitted into the superlattice. If this superlattice is deposited onto a substrate, then reflection off the substrate will occur, and the Brewster condition no longer strictly applies. Even so, one can see that the Brewster modes associated with the ω_{Tm} modes are largely unaffected.

We now turn to the p-polarization results. The analysis is similar to the s-polarization analysis, requiring only some straightforward modifications to Eqs. (32) and (34). The Brewster condition (36) is now replaced by

$$q_x^2=\frac{\omega^2}{c^2}\,\frac{\varepsilon_{xx}-\varepsilon_1\mu_{yy}}{\varepsilon_{xx}/\varepsilon_1-\varepsilon_1/\varepsilon_{zz}}. \tag{37}$$

Figure 3(d) shows the reflectivity spectra for the anisotropy along either x or z. In p polarization, the magnetic component of the EM field interacts with the μ_{yy} only, and this is the same for both these anisotropy directions, resulting in identical spectra. As with the s-polarization results, the spectrum can be understood by reference to the bulk continua and the Brewster mode dispersion shown in Fig. 4(d).

Figure 3(e) shows the reflectivity spectra for the anisotropy along y. Here μ_{yy} is a constant equal to 1, so the superlattice behaves as a dielectric and the spectra are featureless. Figure 4(e) shows the bulk continua and Brewster dispersion curves, which are similarly featureless. In this case the Brewster curve does not represent a ''mode'' in the normal sense since it is not associated with any dispersive effects. It merely represents the conventional ''Brewster angle'' associated with reflection off a dielectric.[41] The angle of incidence (60°) is close to the Brewster angle (66.9°) in this case, which is why the reflectivity is very low.

The appearance of Brewster modes in both s and p polarization contrasts with the case of reflectivity off a nonmagnetic material. In the latter case Brewster modes associated with, for instance, phonon dispersion, appear only in p polarization, so, by analogy, we might expect Brewster modes to appear only in s polarization for the present case, since here we are dealing only with magnon dispersion. In fact, however, Brewster modes also appear in p polarization because, although the dielectric tensor of the superlattice is not dispersive in the region of interest, the material responds to the electric component of an EM field, i.e., the principal components of the superlattice dielectric tensor are not equal to 1.

The above analysis shows that a great deal of information on the superlattice permeability tensor may be obtained from oblique incidence reflection spectroscopy. A possible complementary technique is attenuated total reflection (ATR) spectroscopy. The significance of this technique is that one may get coupling to surface polariton modes which have frequencies dependent on oscillator strengths.[42] For a semi-infinite dielectric in contact with a semi-infinite magnetic superlattice, the s-polarization surface polariton dispersion is given by Eq. (36), although there is now an additional constraint that μ_{xx} must be negative.[4]

The surface polariton dispersion curves following Eq. (36) are shown in Figs. 4(b) and 4(c) as dashed lines. For the system considered, there are no surface polaritons for anisotropy along x or in p polarization.[43] We can thus see that

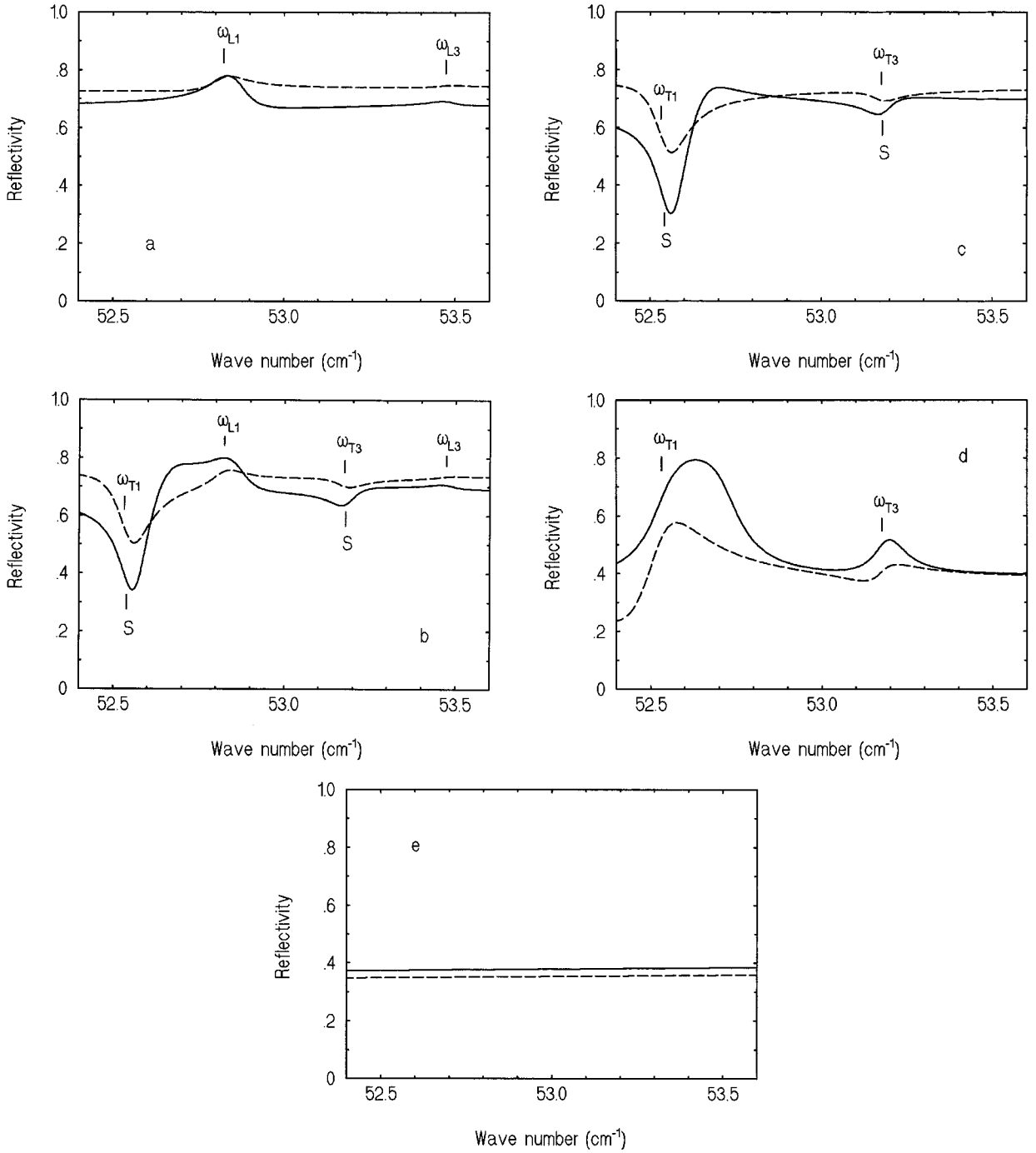

FIG. 5. Calculated 20° silicon ATR spectra of (—) a semi-infinite superlattice and (– – – –) 0.5 μm of superlattice deposited on a semi-infinite substrate. (a) *s* polarization, anisotropy along *x*, (b) *s* polarization, anisotropy along *y*, (c) *s* polarization, anisotropy along *z*, (d) *p* polarization, anisotropy along *x* or *z*, (e) *p* polarization, anisotropy along *y*.

there are considerably fewer surface modes than there are Brewster modes. Where they exist, the surface polariton dispersion curves are extensions of the Brewster mode dispersion curves.

The ATR technique[44] uses a prism separated from the sample by a controlled vacuum gap. The incident beam enters the prism in such a way that it hits the base of the prism at an internal angle greater than the critical angle for total internal reflection. There is then an evanescent field decaying away from the base in the vacuum gap. This field can interact both with the bulk modes in the sample and with the surface polariton field. Dips in the spectra are therefore observed in both of these cases, although the surface polariton dips should be sharper because these modes occur at discrete frequencies, whereas the bulk modes fall in a continuum.

The value of q_x in the ATR experiment is determined by Eq. (35) with ε_1 representing the dielectric constant of the prism material. Figure 4 includes the associated light line when the prism material is silicon ($\varepsilon=11.6$) and the angle of incidence is 20°. As before, the shaded areas correspond to bulk continua, and the unshaded areas to forbidden gaps in which no propagation can occur in the absence of damping.

Thus the ATR experiment for a semi-infinite sample will show higher reflectivities in the forbidden gaps. However, in the presence of damping, this behavior will be modified by the presence of sharp surface mode dips in the reflectivity where the surface polariton dispersion curves intersect the scan line.

The calculated ATR spectra for a semi-infinite superlattice separated from the prism base by 30 μm are shown as solid lines in Fig. 5. The principles summarized above are essentially followed, but we see that the frequencies of the surface mode dips are slightly different from those determined using Eq. (36), marked *S* in the spectra. One particularly noticeable discrepancy observed in Figs. 5(b) and 5(c) is that the calculated dip around ω_{T3} is actually within the bulk continuum. It therefore appears that this minimum has more the character of a Brewster mode between Si and the superlattice than that of a surface mode between vacuum and the superlattice. The exact frequency of the minima are affected by the damping and the vacuum gap. The latter should strictly be infinite for Eq. (36) to be satisfied. If exact information is required from such ATR spectra, it is therefore necessary that either the gap is accurately known or that it is sufficiently large that the effect of the prism on the dip frequency is small.[42]

Figure 5 shows the ATR results for 5 μm of a superlattice deposited on a semi-infinite ZnF_2 substrate as dashed lines. In this case, the surface polariton modes are leaky; they are moved to slightly higher frequency and become broader.

The ATR spectra presented here suggest that the technique may help in investigating the permeability tensor. However one cannot simply rely on dispersion curves to model the frequency of the dips in the spectra; in addition, care must be taken with the vacuum gap. This is in agreement with results found for semiconductor superlattices.[42]

VI. CONCLUSIONS

We have demonstrated a simple way of modeling confined magnon polaritons in superlattices containing antiferromagnets. The permeability tensor may be obtained by straightforward substitution into simple expressions. The calculated spectra also suggest that experimental verification of the form of the permeability tensor should be obtainable using standard techniques.

We expect the analysis to be fairly accurate at low temperatures provided that the superlattice layers are not too thin and that the antiferromagnetic resonances of the two components are not too close in frequency. For our numerical examples, we have considered a superlattice structure that should easily satisfy these criteria. Nevertheless, it would be useful to compare the results of this model with those from a microscopic one, such as that of Stamps and Camley,[21] for structures with shorter periods, in order to investigate the limits at which the present model becomes inapplicable.

In this paper we have only considered a superlattice of two antiferromagnets. In principle, the same method could also be used for other superlattice structures incorporating antiferromagnets, e.g., antiferromagnet/ferromagnet, antiferromagnet/ferrimagnet, or certain antiferromagnet/nonmagnet superlattices. In the last case the applicability of the model depends on the strength of the antiferromagnet anisotropy. The work of Orbach and Pincus[31] suggests that, for layer widths of the order described in this paper, an FeF_2/ZnF_2 superlattice could be reasonably modeled in this way whereas an MnF_2/ZnF_2 superlattice could not.

ACKNOWLEDGMENTS

The authors have benefited from useful discussions with R. L. Stamps, who also provided us with a preprint of Ref. 21. T.D. is supported by the Brazilian agency CAPES.

[1] C. A. Ramos, D. Lederman, A. R. King, and V. Jaccarino, Phys. Rev. Lett. **65**, 2913 (1990).
[2] D. M. Lind, S. D. Berry, G. Chern, H. Mathias, and L. R. Testardi, J. Appl. Phys. **70**, 6218 (1991).
[3] J. A. Borchers, M. J. Carey, R. W. Erwin, C. F. Majkrzak, and A. E. Berkowitz, Phys. Rev. Lett. **70**, 1878 (1993).
[4] N. S. Almeida and D. R. Tilley, Solid State Commun. **73**, 23 (1990).
[5] F. A. Oliveira, Solid State Commun. **78**, 759 (1991).
[6] R. E. Camley, M. G. Cottam, and D. R. Tilley, Solid State Commun. **81**, 571 (1992).
[7] M. C. Oliveros, N. S. Almeida, D. R. Tilley, J. Thomas, and R. E. Camley, J. Phys. Condens. Matter **4**, 8497 (1992).
[8] F. G. Elmzughi, N. C. Constantinou, and D. R. Tilley, Phys. Rev. B **51**, 11 515 (1995).
[9] V. M. Agranovich and V. E. Kravtsov, Solid State Commun. **55**, 85 (1985).
[10] N. Raj and D. R. Tilley, Solid State Commun. **55**, 373 (1985).
[11] B. Jusserand and M. Cardona, in *Light Scattering in Solids V*, edited by M. Cardona and G. Güntherodt (Springer, Berlin, 1989), p. 49.
[12] K. A. Maslin, T. J. Parker, N. Raj, D. R. Tilley, P. J. Dobson, D. Hilton, and C. T. Foxon, Solid State Commun. **60**, 461 (1986).
[13] S. Perkowitz, R. Sudharsanan, K. A. Harris, J. W. Cook, J. F. Schetzina, and J. N. Schulman, Phys. Rev. B **36**, 9290 (1987).
[14] A. R. El-Gohary, T. J. Parker, N. Raj, D. R. Tilley, P. J. Dobson, D. Hilton, and C. T. Foxon, Semicond. Sci. Technol. **4**, 338 (1989).
[15] N. Raj and D. R. Tilley, in *The Dielectric Function of Condensed Matter Systems*, edited by L. V. Keldysh, D. A. Kirzhnitz, and A. A. Maradudin (Elsevier, Amsterdam, 1989), p. 459.
[16] N. Raj and D. R. Tilley, Phys. Rev. B **36**, 7003 (1987).
[17] N. S. Almeida and D. L. Mills, Phys. Rev. B **38**, 6698 (1988).
[18] R. E. Camley, T. S. Rahman, and D. L. Mills, Phys. Rev. B **27**, 261 (1983).
[19] M. Lui, C. A. Ramos, A. R. King and V. Jaccarino, J. Appl. Phys. **67**, 5518 (1990).
[20] B. Samson, T. Dumelow, A. A. Hamilton, T. J. Parker, S. R. P. Smith, D. R. Tilley, C. T. Foxon, D. Hilton, and K. J. Moore, Phys. Rev. B **46**, 2375 (1992).
[21] R. L. Stamps and R. E. Camley, Phys. Rev. B **54**, 15 200 (1996).
[22] T. Dumelow, T. J. Parker, S. R. P. Smith, and D. R. Tilley, Surf. Sci. Rep. **17**, 151 (1993).
[23] T. Dumelow and S. R. P. Smith (unpublished).
[24] D. E. Brown, T. Dumelow, T. J. Parker, Kamsul Abraha, and D. R. Tilley, Phys. Rev. B **49**, 12 266 (1994).

[25] Kamsul Abraha, D. E. Brown, T. Dumelow, T. J. Parker, and D. R. Tilley, Phys. Rev. B **50**, 6808 (1994).
[26] M. R. F. Jensen, T. J. Parker, Kamsul Abraha, and D. R. Tilley, Phys. Rev. Lett. **75**, 3756 (1995).
[27] D. L. Mills and E. Burstein, Rep. Progr. Phys. **37**, 817 (1974).
[28] R. Loudon and P. Pincus, Phys. Rev. **132**, 673 (1963).
[29] E. F. Sarmento and D. R. Tilley, J. Phys. C **10**, 795 (1977).
[30] R. L. Stamps, R. E. Camley, F. C. Nörtemann, and D. R. Tilley, Phys. Rev. B **48**, 15 740 (1993).
[31] R. Orbach and P. Pincus, Phys. Rev. **113**, 1213 (1959).
[32] B. Lüthi, D. L. Mills, and R. E. Camley, Phys Rev. B **28**, 1475 (1983).
[33] L. Remer, B. Lüthi, H. Sauer, R. Geick, and R. E. Camley, Phys. Rev. Lett. **56**, 1190 (1986).
[34] R. W. Sanders, R. M. Belanger, M. Motokawa, V. Jaccarino, and S. M. Rezende, Phys. Rev. B **23**, 1190 (1981).
[35] L. L. Hinchey and D. L. Mills, Phys. Rev. B **33**, 3329 (1986).
[36] R. E. Camley and D. L. Mills, Phys. Rev. B **26**, 1280 (1982).
[37] T. Dumelow and R. E. Camley, Phys. Rev. B **54**, 12 232 (1996).
[38] M. Lui, J. Drucker, A. R. King, J. P. Kotthaus, P. K. Hansma, and V. Jaccarino, Phys. Rev. B **33**, 7720 (1986).
[39] H. Chu and Y-C Chang, Phys. Rev. B **38**, 12 369 (1988).
[40] T. Dumelow and D. R. Tilley, J. Opt. Soc. Am. A **10**, 633 (1993).
[41] F. L. Pedrotti and L. S. Pedrotti, *Introduction to Optics*, 2nd ed. (Prentice-Hall, Englewood Cliffs, NJ, 1993).
[42] A. A. Hamilton, T. Dumelow, T. J. Parker, and S. R. P. Smith, J. Phys. Condens. Matter **8**, 8027 (1996).
[43] R. E. Camley and D. L. Mills, Phys. Rev. B **26**, 1280 (1982).
[44] A. Otto, Z. Phys. **216**, 398 (1968).